Materials Research Express

PAPER

Photoconductivity of bulk $SrTiO_3$ single crystals at room temperature

RECEIVED
3 October 2017

REVISED
27 November 2017

ACCEPTED FOR PUBLICATION
11 December 2017

PUBLISHED
4 January 2018

P Saadatkia[1,2], P Stepanov[1,2] and F A Selim[1,2]

[1] Center for Photochemical Sciences, Bowling Green State University, Bowling Green, OH 43403, United States of America
[2] Department of Physics and Astronomy, Bowling Green State University, Bowling Green, OH 43403, United States of America

E-mail: faselim@bgsu.edu

Keywords: photoconductivity, $SrTiO_3$, positron annihilation spectroscopy, defects

Abstract

Room temperature photoconductivity measurements have been carried out on various as-grown $SrTiO_3$ single crystals provided from different suppliers. We observed an increase in the conductivity of samples based on photon energy and photon intensity. While low energy photons decreased the conductivity, photons with energy close to the band gap of $SrTiO_3$ enhanced the conductivity. No persistent photoconductivity was observed in these samples. Defects play the main role in inducing the photoconductivity. Positron annihilation lifetime spectroscopy and digital coincidence Doppler broadening spectroscopy were used to investigate the presence and nature of defects in the photoconductive samples. The measurements revealed high concentration of defects and the dependence of photoconductivity on defect concentration under 365 and 400 nm illumination.

1. Introduction

$SrTiO_3$ (STO) is one of the members of perovskite family which has potential applications in electronic industries including oxygen sensors [1] capacitors, tunable microwave devices [2, 3] because of its high dielectric constants [4]. It shows unusual electronic transport behavior due to the dependency of its dielectric constant on electric field and temperature [5]. At room temperature, it has a cubic structure which goes through well-known structural phase transition from cubic to tetragonal at 105 K due to the opposite rotation of neighboring oxygen octahedra [6]. STO is a wide bang gap semiconductor with band gap of 3.2 eV [7] and it can be tuned to a conductor by doping [8].

Recently, formation of 2D electron gas has been observed at the interface of STO and LAO which opens a new window for future multifunctional oxide electronic devices [9, 10]. This phenomenon has been explained in different ways, it could be related to polar discontinuity, oxygen vacancies as well as La diffusion since both La and oxygen vacancies can act as donors to the interface. Additionally, persistent photoconductivity was reported on STO/LAO interfaces with about 4 orders of magnitude [11]. Later, persistent photoconductivity was also observed in Bulk annealed STO single crystals [12].

In the present work, Hall and photo Hall measurements have been carried out on a number of as-grown STO samples provided from different suppliers to investigate the photo-response of bulk STO and its dependence on photon energy and intensity. Also, positron annihilation lifetime spectroscopy and digital coincidence Doppler broadening spectroscopy were applied to examine the presence of defects and their role on the photoconductivity of STO single crystals.

2. Experimental

Light emitting diodes (LEDs) of different wavelengths (365, 400, 460, 650 nm) were used for photo Hall measurements on as-grown STO single crystals at room temperature. The crystals were purchased from different providers; however, they are all (100) and grown by the flame diffusion method (Verneuil process). A MMR Hall system has been customized for photo Hall measurement, where a window has been built into the chamber for sample illumination. Another important characteristic of our Hall-effect system used in this

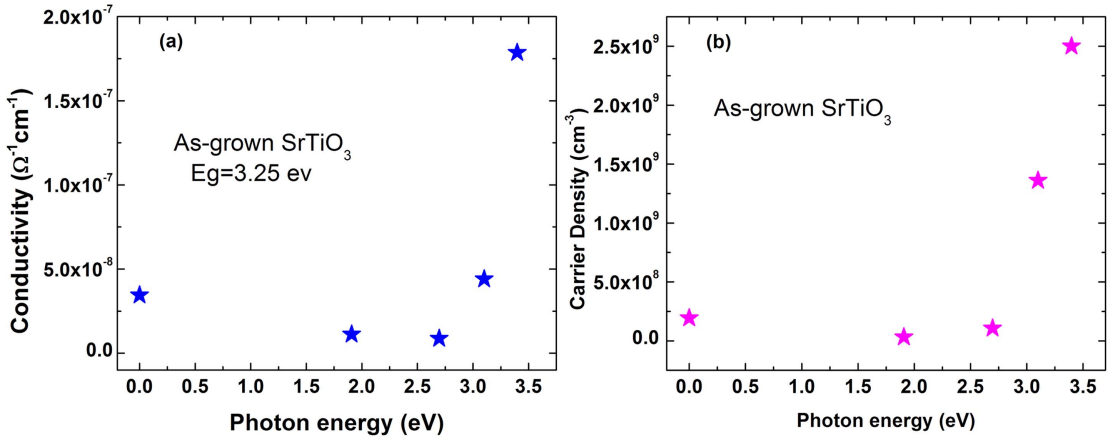

Figure 1. Dependence of (a) conductivity and (b) carrier density on photon energy at room temperature.

experiment is the precise control of the sample temperature during the measurements. The samples were cooled down during the measurements and the temperature was stabilized to avoid heating the sample during the photo illumination. Indium contacts were mounted on the surface of each sample.

Positron annihilation lifetime spectroscopy and digital coincidence Doppler broadening spectroscopy were employed for defect analysis. Positron annihilation lifetime spectroscopy measurements were carried out using a conventional analog positron coincidence spectrometer [13] with two BaF_2 detectors. The detectors are positioned in collinear geometry and the instrumental resolution of the system is about 300 ps. The theoretical positron lifetime spectrum (sum of exponential components) is convoluted with the resolution function (Gaussian). Therefore, the resolution function does affect the shape of the spectrum in a certain way (broadens the spectrum). But when we fit the experimental spectrum with the corresponding convoluted model we still can extract components with lifetimes less than the width of the resolution function. This resolution range of 200–300 ps and the extracted lifetime components in the range of 100 ps are common in positron lifetime measurements [14]. The positron source used in the experiment was made from a 30 μCi ^{22}Na isotope sealed in between two layers of an 8 μm thick Kapton foil. The source was sandwiched between two identical STO samples. To have good statistics, in each lifetime spectrum several million counts were recorded. Basically, each spectrum is a superposition of exponential decay components convoluted with three Gaussian functions denoted the instrumental resolution function. The source contribution due to positron annihilation inside the Kapton foil was about 12%.

In Doppler broadening measurements two high purity Ge detectors are simultaneously registering a pair of 511 keV photons due to positron annihilation with valence and core electrons inside the material under investigation. Energy resolution of the system is 1.2 keV at photon energy of about 0.5 MeV. The shape of the Doppler spectra is depicted by the line-shape S and W parameters, which represent the fraction of positrons that annihilate with valence and core electrons respectively [15–17].

3. Results and discussion

3.1. Photo induced effects on the electrical transport properties of STO

Figure 1 presents the dependence of conductivity and carrier concentration on photon energies at room temperature. STO single crystals were provided by MTI Inc. Dark conductivity and carrier density are $3.45 \times 10^{-8}\,\Omega^{-1}\,\mathrm{cm}^{-1}$ and $1.93 \times 10^{8}\,\mathrm{cm}^{-3}$ respectively which increased one order of magnitude under 365 nm (corresponding 3.4 eV) illumination. The crystals exhibit an increase in conductivity only upon illumination with light with energy higher than 3.1 eV (400 nm). This can be due to light induced shallow donors which greatly enhances the conductivity. By comparing figures 1(a) and (b), it can be seen that the induced photoconductivity is totally dependent on the increase of carrier concentrations. Katsu *et al* [18] have reported giant photoconductivity in STO below 105 K (where phase transition occurs) under the light of a wavelength shorter than 400 nm while we observed this phenomenon here at room temperature.

Figure 2 shows photoconductivity of as-grown STO single crystals as a function of illumination intensity with 365 and 400 nm measured by Van der Pauw technique. Fitting of data using $\sigma = AI^{\alpha}$ equation where σ is conductivity, A a constant, I illumination intensity and α the exponent of intensity yields values of α as 0.82 and 1.09 under 400 and 365 nm illumination respectively. In order to estimate the photon intensity, equation

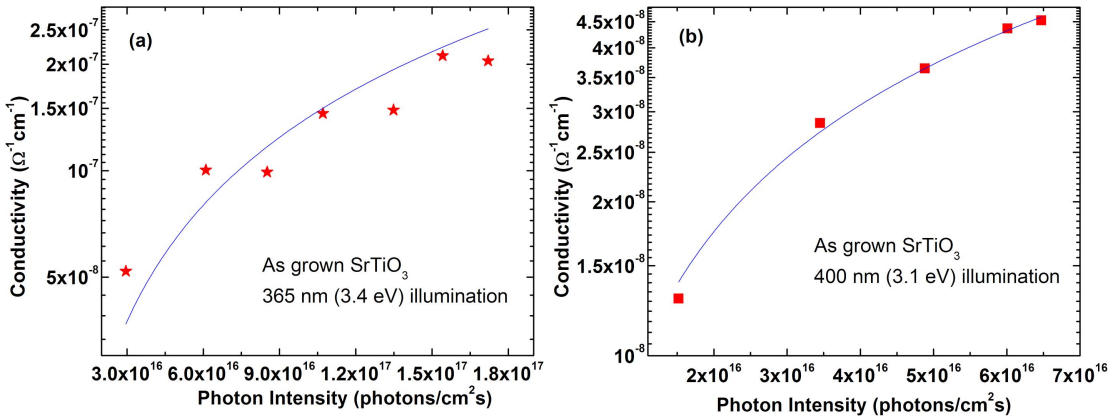

Figure 2. Dependence of conductivity on photon intensity at room temperature under (a) 365 nm (b) 400 nm illumination.

$I = C(\lambda)P$ was applied where I is the illumination intensity in photons cm^{-2} s^{-1}, P power in mW cm^{-2} and C a constant with different values depending on illumination wavelength. The graphs in figures 2(a) and (b) do not indicate saturation up to 10^{17} photons cm^{-2} s^{-1} photon intensity. Illumination with higher light intensity is not possible with our current photoconductivity setup. Thermally stimulated measurements on this sample confirmed the presence of high level of traps in the band gap [19].

3.2. Origin of photoconductivity and role of defects

Investigating the electrical properties of bulk STO is critical to understand interesting phenomena such as persistent photoconductivity [12], transient photoconductivity as well as anomalous photoconductivity occurred during phase transition of STO [18]. Due to high resistivity of undoped STO, more studies of electrical properties have been reported on doped STOs compared to as-grown ones. P-type photoconductivity has been observed in annealed STO single crystals by Poole *et al* which has been suggested to attribute to the same acceptors (V_{Ti}–V_O) that cause the persistent photoconductivity in STO [20]. Temperature dependent conductivity of STO also has been studied widely [18, 21, 22] which shows fascinating results where structural phase transition happens in STO. For instance, Zhang *et al* reported unusual ultraviolet photoconductivity in STO which makes it ultraviolet-sensitive below 105 K, the reason behind this behavior is the transformation of indirect bandgap to the direct bandgap determined by the structural phase-transition of STO [22].

In the present work, photoconductivity measurements were performed at room temperature on several as-grown STO single crystals provided from different suppliers. We named the samples according to the provider company as MTI, University wafer, coating & crystal a, and coating & crystal b. Samples were illuminated under 365 and 400 nm LEDs. Figure 3 indicates the conductivity, carrier density and Hall coefficient of four as-grown STO samples under 365 nm illumination. Photoconductivity curves for MTI and university wafer samples are nearly the same, showing dark conductivity of $1.74 \times 10^{-8}\,\Omega^{-1}\,\mathrm{cm}^{-1}$ and $1.57 \times 10^{-8}\,\Omega^{-1}\,\mathrm{cm}^{-1}$ respectively while coating & crystal a and b samples are more resistive ($3.52 \times 10^{-9}\,\Omega^{-1}\,\mathrm{cm}^{-1}$ and $9.03 \times 10^{-9}\,\Omega^{-1}\,\mathrm{cm}^{-1}$ respectively). MTI and university wafer samples show higher photoconductivity than the other two samples.

The carrier concentration and Hall coefficient curves correlate with photoconductivity results showing the same trend for all the samples. Table 1 summarizes the dark and photocarrier density and photoconductivity at the maximum current of 365 nm LED. The correlation between the increase in carrier density and photoconductivity will be discussed in detail after table 2.

Same experiment was carried out on samples using 400 nm LED for illumination (figure 4). The measurements indicate different trends at low intensities under 400 nm illumination compared to when 365 nm LED was applied. It is noted that conductivity of all samples dropped at very low intensities which could be explained as follows. Illuminating samples with light may either increase the carrier concentration that enhances the conductivity, or change the charge state of defects which may lead to the increase of scattering centers in the samples and consequently hindering conductivity. Considering figure 4, it is obvious that even though the carrier concentration of all samples increased under 400 nm illumination, creation of scattering centers is more dominating in decreasing the conductivity at low intensities.

University wafer sample reveals much more pronounce (5 times) improvement in conductivity along with three orders of magnitude increase in carrier density while MTI is not photoconductive under 400 nm illumination (figure 4). Corresponding results are summarized in table 2. By inspecting tables 1 and 2, it can be seen that carrier density in all the samples increased few orders of magnitude more than photoconductivity after illumination under 365 and 400 nm compare to dark values. The less increase in conductivity compare to carrier

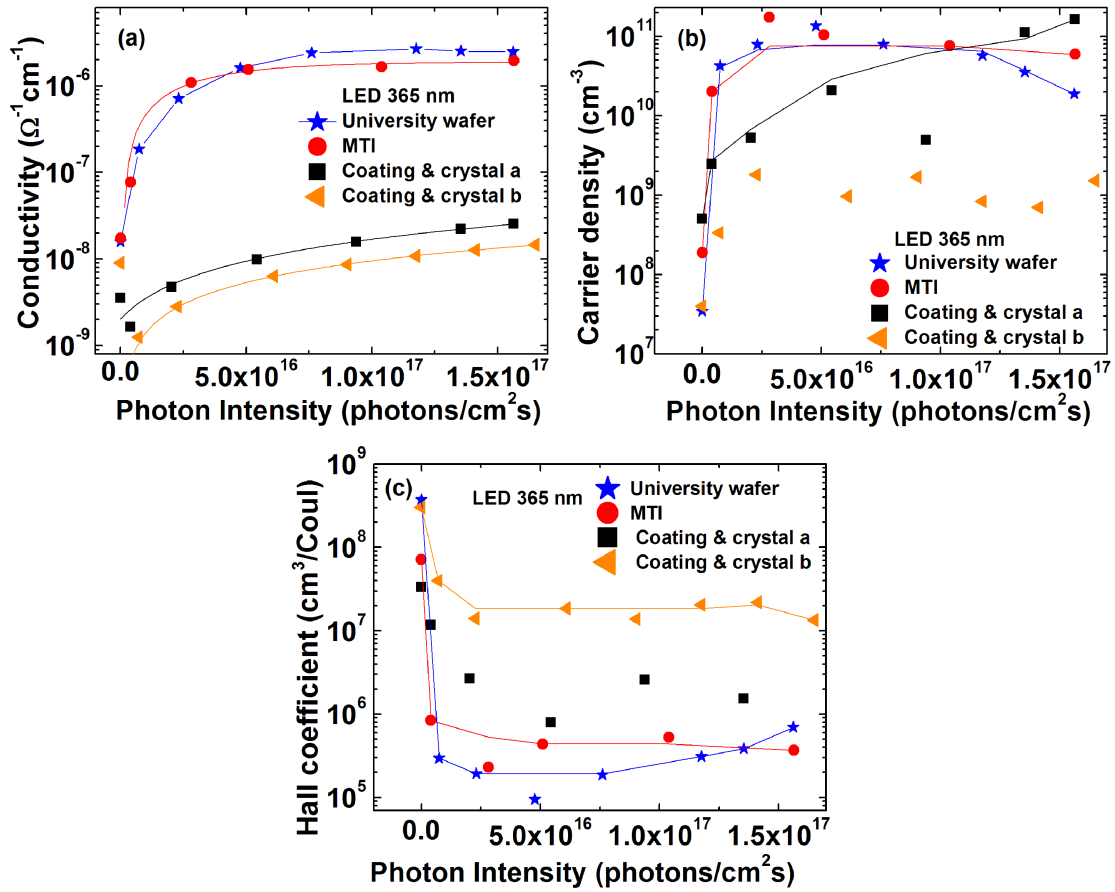

Figure 3. Dependence of (a) conductivity (b) carrier density and (c) Hall coefficient of different as-grown STO on photon intensity under 365 nm illumination.

Table 1. Dark and photoconductivity, dark and photocarrier density of four different as-grown STOs using the maximum current of 365 nm LED.

Samples	Dark conductivity (Ω^{-1} cm^{-1})	Photoconductivity (Ω^{-1} cm^{-1})	Dark carrier density (cm^{-3})	Photocarrier density (cm^{-3})
MTI	1.74×10^{-8}	1.96×10^{-6}	1.87×10^{8}	5.94×10^{10}
University wafer	1.57×10^{-8}	2.5×10^{-6}	3.46×10^{7}	1.89×10^{10}
Coating & crystal a	3.52×10^{-9}	2.56×10^{-8}	4.95×10^{8}	1.63×10^{11}
Coating & crystal b	9.03×10^{-9}	1.46×10^{-8}	3.99×10^{7}	1.53×10^{9}

Table 2. Dark and photoconductivity, dark and photocarrier density of four different as-grown STOs using the maximum current of 400 nm LED.

Samples	Dark conductivity (Ω^{-1} cm^{-1})	Photoconductivity (Ω^{-1} cm^{-1})	Dark carrier density (cm^{-3})	Photocarrier density (cm^{-3})
MTI	2.39×10^{-8}	1.65×10^{-8}	5.39×10^{8}	1.41×10^{10}
University wafer	1.43×10^{-8}	5.63×10^{-8}	8.54×10^{7}	6.98×10^{10}
Coating & crystal a	2.20×10^{-8}	3.70×10^{-8}	5.06×10^{8}	3.73×10^{10}
Coating & crystal b	1.57×10^{-8}	1.93×10^{-8}	3.56×10^{7}	1.97×10^{10}

concentration could be due to the effect of light on inducing scattering centers which may hinder the electron mobility.

Different types and concentration of defects could be behind the difference in photoconductivity of as-grown STO samples which requires further investigation specially when sub band gap light was used as

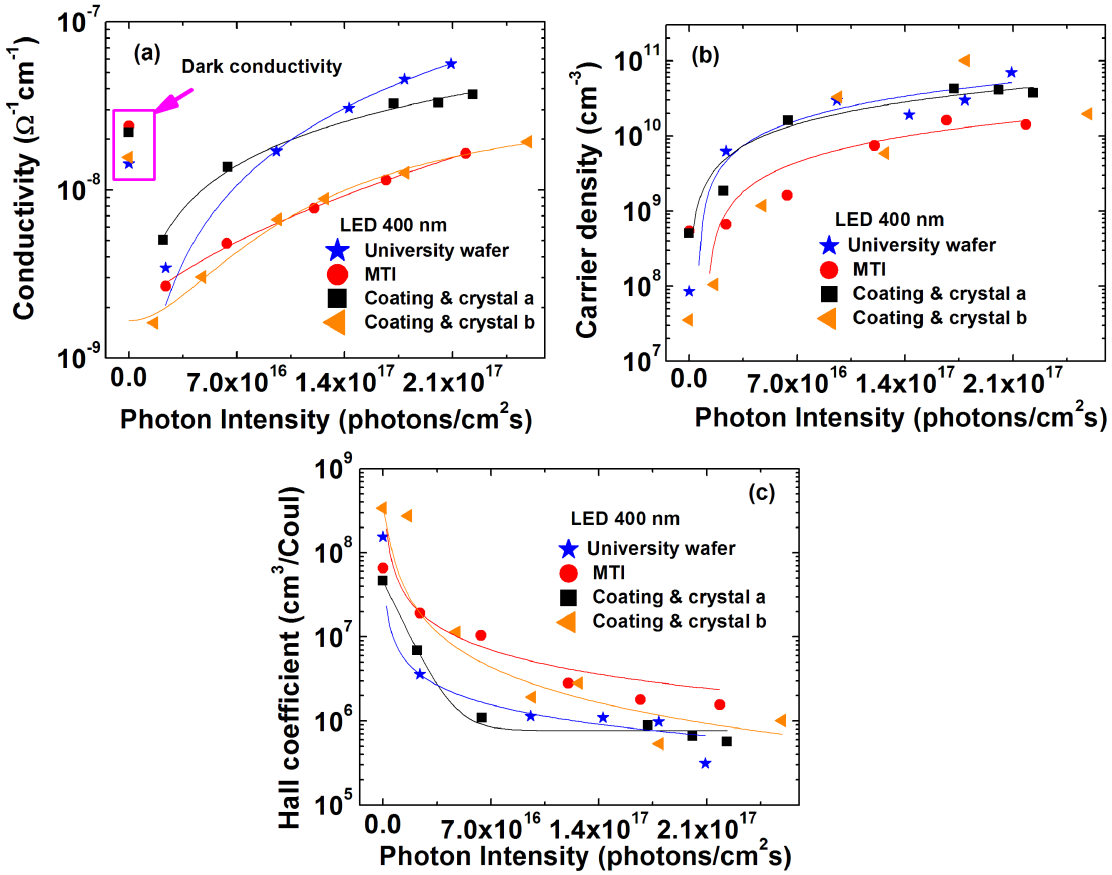

Figure 4. Dependence of (a) conductivity and (b) carrier density and (c) Hall coefficient of different as-grown STO on photon intensity under 400 nm illumination.

Table 3. Positron lifetime data for different STO single crystals which represents average lifetime ($\bar{\tau}$), bulk lifetime (τ_{bulk}), first defect lifetime (τ_{d1}), second defect lifetime (τ_{d2}), intensity of first defect lifetime I_2, first defect trapping coefficient (κ_{d1}), second defect trapping coefficient (κ_{d2}) and goodness of fit (χ^2).

Sample	$\bar{\tau}$, ps	τ_{bulk}, ps	τ_{d1}, ps	I_2(%)	K_{d1}, ns^{-1}	τ_{d2}, ps	K_{d2}, ns^{-1}	χ^2
MTI	141.6	138 ± 4	151.5 ± 1.7	81.8	2.64 ± 0.07	—	—	1.021 ± 0.007
University wafer	183.8	140.3 ± 0.2	179.36 ± 0.09	92.6	104.23 ± 0.09	298 ± 2	6.8107 ± 0.0014	1.015 ± 0.011
Coating & crystal a	169.8	127.1 ± 1.9	172.84 ± 0.08	98.2	110.78 ± 0.15	—	—	0.991 ± 0.007
Coating & crystal b	174.1	140 ± 5	175.35 ± 0.09	99.3	192.6 ± 1.6	—	—	1.044 ± 0.012

illumination source. Generally, identifying defects in STO [23] and other transition metal oxides is crucial to determine various properties of the material like electrical conductivity and domain stability [24, 25]. Positron annihilation lifetime spectroscopy is an excellent technique to identify vacancy-related point defects in materials on atomic scale since positrons tend to localize at open-volume defects [26–29]. Moreover, it provides information about different types of defects and their concentrations in the material. Positron lifetime data were fitted using LT10 [30] and the results are summarized in table 3.

Two and three-state trapping model were used to fit the positron lifetime data. Average lifetimes of the samples vary between 142 and 184 ps. Average lifetimes can be determined by $\bar{\tau} = \sum_i I_i \tau_i$ where τ is the lifetime and I is the probability of annihilating positron in the corresponding state [31]. Basically, by comparing average lifetime and bulk lattice lifetime (if $\bar{\tau} > \tau_{bulk}$) one can measure the vacancy type defects in the material. κ_d is trapping coefficient which indicates the rate of positron trapping to the vacancy and is related to defect concentration [d], based on one defect trapping model or two-state trapping model [13, 31],

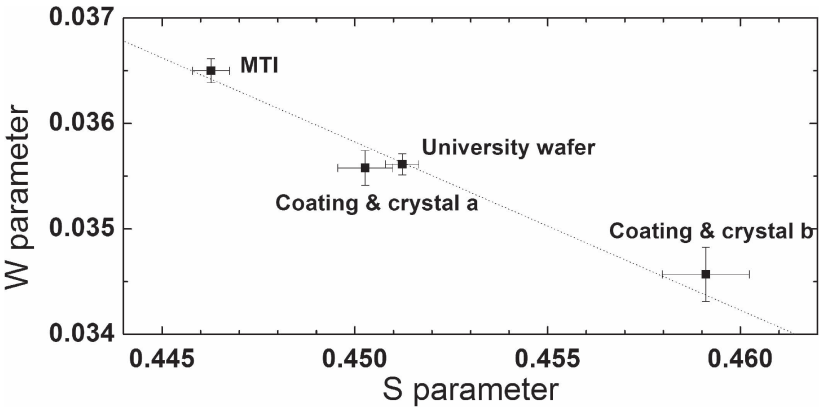

Figure 5. *S* and *W* parameter for four different as-grown STO samples.

$$\kappa_d = \mu_d[d] = I_2\left(\frac{1}{\tau_1} - \frac{1}{\tau_2}\right), \tag{1}$$

where τ_2 is the defect lifetime (τ_{d1})and τ_1 is lifetime which is reduced from the bulk lifetime rely on trapping coefficient,

$$\frac{1}{\tau_1} = \frac{1}{\tau_{\text{bulk}}} + \kappa_d. \tag{2}$$

The intensity of defect lifetime I_2 increases and getting close to unity by increasing defect concentration [31].

Earlier positron lifetime measurements on STO allow us to easily interpret data [31, 32]. Positron lifetime in the bulk material for all samples resides within the range of 130–140 ps (table 3). First sample has the lowest defect lifetime (150 ps) which is very close to the bulk lifetime. Reference [31] reported that this short lifetime is associated with presence of oxygen vacancies which do not act as effective traps for positron. The other three samples have a very high concentration of defects with a consistent lifetime of 170–180 ps [31]. This is a typical value for a titanium vacancy. The primary interest evidenced by table 3 is the longer lifetime STO samples have, the more photoconductivity they reveal under 400 nm illumination (3.1 eV). Also, MTI sample with shortest lifetime, has different type of defects and does not show photoconductivity under 400 nm illumination. It is also interesting to observe the high trapping coefficient (which correspond to high defect concentration) of coating & crystal b sample, this could be the reason behind showing less photoconductivity under 365 nm illumination compared to other samples. Although 365 nm (3.4 eV) photons have larger energy than band gap energy of STO, high defect concentration can cause more scattering of the carriers and decrease in photoconductivity.

Figure 5 shows the *W* versus *S* parameter plot for STO samples. The Doppler data is in a good agreement with the positron lifetime results. MTI sample which is not photoconductive under 400 nm illumination has the shortest lifetime and lowest *S* parameter which indicates the lowest concentration of defects. The university wafer and coating & crystal (a) samples demonstrate higher fraction of annihilation events with the valence electrons which results in the higher *S* values. Coating & crystal (b) sample has the highest defect concentrations as indicated from *S*-parameter and lifetime measurements. These three samples with high concentration of defects show high level of photoconductivity under 400 nm illumination illustrating the significant role of defects in inducing photoconductivity.

4. Conclusions

The effect of photon energy and photon intensity on the electrical conductivity of as-grown STO single crystals were investigated under different illumination at room temperature. Samples became photoconductive when photons with energies close to the band gap and higher were used for illumination. Photoconductivity measurements were performed on several as-grown STOs under 365 and 400 nm illumination. Most of samples were photoconductive at room temperature but no persistent photoconductivity was observed. Vacancy defects were suggested to be behind the photoconductivity phenomena at room temperature. Based on positron life time spectroscopy and coincidence Doppler broadening spectroscopy, we identified a high concentration of defects in the band gap which strongly correlate with the photoconductivity measurements. Ti-vacancy seems to be the source of photoconductivity in most samples. The work also showed that the level of defects and induced photoconductivity is sensitive to the growth conditions.

ORCID iDs

F A Selim https://orcid.org/0000-0001-8367-3785

References

[1] Voigts F, Damjanovic T, Borchardt G, Argirusis C and Maus-Friedrichs W 2006 *J. Nanomater.* **2006** 63154
[2] Kozyrev A *et al* 1995 *Microelectron. Eng.* **29** 257
[3] Gevorgian S, Carlsson E, Wikborg E and Kollberg E 1998 Tunable microwave devices based on bulk and thin film ferroelectrics *Integr. Ferroelectr.* **22** 245
[4] Hemberger J, Lunkenheimer P, Viana R, Böhmer R and Loidl A 1995 *Phys. Rev.* B **52** 13159
[5] Viana R, Lunkenheimer P, Hemberger J, Böhmer R and Loidl A 1994 *Phys. Rev.* B **50** 601
[6] Cowley R 1996 *Phil. Trans. R. Soc.* A **354** 2799
[7] Bieger T, Maier J and Waser R 1992 *Solid State Ion.* **53** 578
[8] Ishida Y *et al* 2008 *Phys. Rev. Lett.* **100** 056401
[9] Herranz G, Sanchez F, Dix N, Scigaj M and Fontcuberta J 2012 *Sci. Rep.* **2** 758
[10] Ohtomo A and Hwang H 2004 *Nature* **427** 423
[11] Tebano A, Fabbri E, Pergolesi D, Balestrino G and Traversa E 2012 *ACS Nano* **6** 1278
[12] Tarun M C, Selim F A and McCluskey M D 2013 *Phys. Rev. Lett.* **111** 187403
[13] Krause-Rehberg R and Leipner H S 1999 *Positron Annihilation in Semiconductors: Defect Studies* (Berlin: Springer)
[14] Selim F A, Varney C, Tarun M C, Rowe M, Collins G and McCluskey M D 2013 *Phys. Rev.* B **88** 174102
[15] Hautojärvi P 1979 *Positrons in Solids* (Berlin: Springer)
[16] Selim F A, Wells D P, Harmon J F, Kwofie J, Lancaster G and Jones J L 2003 *AIP Conf. Proc.* **680** 499
[17] Selim F A, Wells D P, Harmon J F and Williams J 2005 *J. Appl. Phys.* **97** 113539
[18] Katsu H, Tanaka H and Kawai T 2000 *Japan. J. Appl. Phys.* **39** 2657
[19] Wang B, Saadatkia P, Selim F and Look D 2017 Study of trapping phenamena in $SrTiO_3$ by thermally stimulated techniques *J. Electron. Mater.* **47** 604-11
[20] Poole V M, Corolewski C D and McCluskey M D 2015 P-type conductivity in annealed strontium titanate *AIP Adv.* **5** 127217
[21] Rossella F, Galinetto P, Samoggia G, Trepakov V and Jastrabik L 2007 *Solid State Commun.* **141** 95–8
[22] Zhang H, Yan L and Habermeier H 2012 Unusual ultraviolet photoconductivity in single crystalline $SrTiO_3$ *J. Phys.: Condens. Matter* **25** 035802
[23] Jupille J and Thornton G 2015 *Defects at Oxide Surfaces* (Berlin: Springer)
[24] Smyth D M 2000 *The Defect Chemistry of Metal Oxides* (Oxford: Oxford University Press)
[25] Damjanovic D 1998 Ferroelectric, dielectric and piezoelectric properties of ferroelectric thin films and ceramics *Rep. Prog. Phys.* **61** 1267
[26] Fieschi R, Gainotti A, Ghezzi C and Manfredi M 1968 *Phys. Rev.* **175** 383
[27] Selim F, Weber M, Solodovnikov D and Lynn K 2007 *Phys. Rev. Lett.* **99** 085502
[28] Tuomisto F, Ranki V, Saarinen K and Look D C 2003 *Phys. Rev. Lett.* **91** 205502
[29] Keeble D, Wicklein S, Dittmann R, Ravelli L, Mackie R and Egger W 2010 *Phys. Rev. Lett.* **105** 226102
[30] Giebel D and Kansy J 2012 *Phys. Proc.* **35** 122
[31] Mackie R, Singh S, Laverock J, Dugdale S and Keeble D 2009 *Phys. Rev.* B **79** 014102
[32] Selim F, Winarski D, Varney C, Tarun M, Ji J and McCluskey M 2015 *Results Phys.* **5** 28